




Effects of external electric and magnetic field on the nonlinear optical rectification, second, and third-harmonic generations in GaAs/AlGaAs asymmetric triple quantum well

A. Turker Tuzemen^{1,a} , E. B. Al^{2,b}, H. Dakhlaoui^{3,4,c}, F. Ungan^{2,d}

¹ Department of Mathematics and Science Education, Faculty of Education, Sivas Cumhuriyet University, 58140 Sivas, Turkey

² Department of Physics, Faculty of Science, Sivas Cumhuriyet University, 58140 Sivas, Turkey

³ Nanomaterials Technology Unit, Basic and Applied Scientific Research Center (BASRC), College of Science of Dammam, Imam Abdulrahman Bin Faisal University, P. O. Box 1982, 31441 Dammam, Saudi Arabia

⁴ Department of Physics, College of Sciences for Girls, Imam Abdulrahman Bin Faisal University, Dammam, Saudi Arabia

Received: 8 May 2023 / Accepted: 20 July 2023

© The Author(s), under exclusive licence to Società Italiana di Fisica and Springer-Verlag GmbH Germany, part of Springer Nature 2023

Abstract In this paper, we theoretically investigate the nonlinear optical rectification (NOR), second-harmonic generation (SHG), and third-harmonic generation (THG) coefficients of an AlGaAs/GaAs asymmetric triple quantum well structure under external electric and magnetic fields. To do this, we first obtain the solution of the time-independent Schrödinger equation numerically using the diagonalization method under the effective mass approximation to obtain the subband energy levels (with related wave functions) of the heterostructure. We then use the compact density matrix method to form the mathematical expressions of NOR, SHG and THG coefficients. The numerical results from our investigation show that the resonance peaks of the NOR, SHG and THG coefficients shift to a high energy (low energy) region with an increase in the magnitude of the electric (magnetic) field. As a result, we believe that numerical results obtained from carried out our parameter analyzes will present important developments and provide great contributions in designing new optoelectronic devices related asymmetric triple quantum well structure.

1 Introduction

In semiconductor heterostructures, the nonlinear optical properties related to intersubband transitions are important for obtaining optoelectronic devices with desired features, such as light emitting diodes [1], laser diodes [2], photodetectors [3], and photodiodes [4]. Such properties of heterostructures, including quantum wells (QWs), quantum well wires (QWWs), and quantum dots (QDs), form the physical foundation of optoelectronic devices in today's technology. QWs are more preferred structures than other heterostructures, as they have mathematical computational advantages in addition to a wide band gap and ease of production. Furthermore, the probability of fabricating new devices in electronics and optoelectronics is quite high with QW structures. The physical properties of a QW can be controlled by applying external fields to the structure, such as electric fields, magnetic fields, and intense laser fields [5–7]. As a result of the application of electric and magnetic fields, significant changes in the electron energy spectrum can occur in QW heterostructures. These changes affect many features of the structure. For example, by applying a static electric field to the heterostructure, strong nonlinear optical responses can be obtained by increasing the expected values of the electron dipole moment. Alternatively, when a magnetic field is applied to the structure, carrier confinement increases, leading to the formation of discrete energy levels. In low-dimensional heterostructures, nonlinear optical properties such as SHG, NOR, and THG are quite important for the applications of optoelectronic devices in technology [8–13]. Consequently, interest in nonlinear optical properties has increased from the past to the present, and many studies have been conducted on this subject. Aytikin et al. [14] studied the Pöschl-Teller QW and investigated the nonlinear optical properties of the heterostructure under electric and magnetic fields. They showed that the electric field increased and the magnetic field decreased the values of the nonlinear coefficients. Mora-Ramos et al. [15] examined the linear and nonlinear properties of a GaAs-Ga_{0.7}Al_{0.3}As single QW under the effects of applied electric and magnetic fields. According to their results, it was revealed that external fields significantly affect all features of the structure. In another work, Liu et al. [16] determined the effects of hydrostatic pressure, temperature, and magnetic field on the NOR and SHG for an asymmetrical Gaussian potential QW. They found that while the resonant peaks of the NOR coefficients and SHG susceptibility

^a e-mail: atuzemen@cumhuriyet.edu.tr (corresponding author)

^b e-mail: emrebahadiral@hotmail.com

^c e-mail: h_dakhlaoui@yahoo.fr

^d e-mail: fungan@cumhuriyet.edu.tr

have redshift under the applied hydrostatic pressure and temperature, the resonant peaks shift to the red end when a magnetic field was applied. Restrepo et al. [17] investigated how the SHG and THG coefficients in a Morse potential QW were changed under the effects of electric and magnetic fields. They concluded that the resonant peak positions (shift to blue) and magnitudes of SHG and THG coefficients were significantly affected by the presence of both electric and magnetic fields. Other studies discussed the influences of applied external fields, such as electric, magnetic, and laser fields, on the nonlinear optical properties of Woods-Saxon potential QWs and Konwent potential QWs, done by Ungan et al. [18] and Sayrac et al. [19], respectively.

In this study, we investigate the nonlinear optical properties of an asymmetric triple quantum well (QW) structure with three different bottom potential profile shapes made of GaAs/Al_{0.3}Ga_{0.7}As under the influence of external electric and magnetic fields. We examine the changes in the NOR, SHG, and THG coefficients under external fields. The subband energy levels (with wave functions) and the mathematical expressions of the NOR, SHG, and THG coefficients are obtained using diagonalization and compact density matrix methods. The paper is organized as follows: Sect. 2 describes the problem and its solution, Sect. 3 presents the obtained results and comments on them, and Sect. 4 provides the conclusions.

2 Theory

In this part of the study, the computation of the electron subband energy levels and corresponding wave functions with the effects of external fields will be presented for the GaAs/Al_{0.3}Ga_{0.7}As asymmetric triple QWs heterostructure which has three different bottom potential profile shapes. Additionally, details on how the equations for NOR, SHG, and THG coefficients are obtained will be provided. The z -axis represents the growth direction of the heterostructure. The electric field (\mathbf{F}) and magnetic field (\mathbf{B}) are oriented parallel $(0, 0, F)$ and perpendicular $(B, 0, 0)$ to the growth direction of the structure, respectively. The Hamiltonian for the motion of the confined electron in the effective mass and parabolic band approximations, taking into account the applied external fields, is given by [13, 20]

$$H = -\frac{1}{2m^*} \left(\mathbf{P} + \frac{e}{c} \mathbf{A}(\mathbf{r}) \right)^2 + V(z) + |e|Fz \quad (1)$$

where m^* and e shows the effective mass and the elementary charge of electron, respectively. While \mathbf{P} represents the momentum operator, c denotes the light's speed in free space. The Landau gauge is given by $\mathbf{A}(\mathbf{r}) = -Bz\hat{y}$. F expresses the intensity of the electric field. Finally, $V(z)$ is the confined potential of the structure and given by

$$V(z) = \begin{cases} \frac{2}{L_L^2} \left(z + b_L + \frac{(L_M+L_L)}{2} \right)^2 V_0 & -\left(L_L + b_L + \frac{L_M}{2} \right) \leq z \leq -\left(b_L + \frac{L_M}{2} \right) \\ \left(-\frac{2}{L_M^2} z^2 + \frac{1}{2} \right) V_0 & -\frac{L_M}{2} \leq z \leq 0 \\ \left(\frac{2}{L_M^2} z^2 \right) V_0 & 0 \leq z \leq \frac{L_M}{2} \\ \left(-\frac{2}{L_R^2} \left(z - b_R - \frac{(L_M+L_R)}{2} \right)^2 + \frac{1}{2} \right) V_0 & \frac{L_M}{2} + b_R \leq z \leq \frac{L_M}{2} + b_R + L_R \\ V_0 & \text{elsewhere} \end{cases} \quad (2)$$

here V_0 and $L_L = L_M = L_R$ show the depth and the width of the each QW, respectively. Besides b_L and b_R represent left barrier width and right barrier width.

Firstly, we solved the one-dimensional time-independent Schrödinger equation using the diagonalization method [21], which involves expressing the electron's wavefunctions $\Psi(z)$ in terms of a complete set of orthonormal functions of an infinite barrier potential well, as explained in [17, 22, 23]. This allowed us to obtain the subband energy levels and corresponding wave functions ($H\Psi(z) = E\Psi(z)$), where E represents the energy eigenvalues. The data obtained from these calculations provided us with information about intersubband transitions and dipole matrix elements related to the subbands. Subsequently, we used the compact density matrix method [12, 24–26] to derive the mathematical expressions for NOR, SHG, and THG, which are written below, respectively,

$$\chi_0^{(2)} = \frac{4e^3 \rho_v}{\varepsilon_0 \hbar^2} \mu_{01}^2 \delta_{01} \frac{\omega_{10}^2 (1 + \Gamma_2 / \Gamma_1) + (\omega^2 + \Gamma_2^2) (\Gamma_2 / \Gamma_1 - 1)}{[(\omega_{10} - \omega)^2 + \Gamma_2^2][(\omega_{10} + \omega)^2 + \Gamma_2^2]} \quad (3)$$

$$\chi_{2\omega}^{(2)} = \frac{e^3 \rho_v}{\varepsilon_0 \hbar^2} \frac{\mu_{01} \mu_{12} \mu_{20}}{(\omega - \omega_{10} - i\Gamma_3)(2\omega - \omega_{20} - i\Gamma_3)} \quad (4)$$

$$\chi_{3\omega}^{(3)} = \frac{e^4 \rho_v}{\varepsilon_0 \hbar^3} \frac{\mu_{01} \mu_{12} \mu_{23} \mu_{30}}{(\omega - \omega_{10} - i\Gamma_3)(2\omega - \omega_{20} - i\Gamma_3)(3\omega - \omega_{30} - i\Gamma_3)} \quad (5)$$

In the set of Eqs. (3–5), while ρ_v denotes the concentration of electrons in three dimensions, ϵ_0 and \hbar are the permittivity of vacuum and the reduced Planck constant, respectively. μ_{ij} state the dipole matrix elements $\mu_{ij} = \Psi_i |z| \Psi_j$, ($i, j = 0, 1, 2, 3$) ($\delta_{01} = |\mu_{00} - \mu_{11}|$). The transition frequency is given as $\omega_{ij} = (E_i - E_j)/\hbar$. The relaxation rate related to transition lifetime of the electrons is given by the expression, $\Gamma_k = 1/T_k$ ($k = 1, 2, 3$).

In this investigation, the numerical values of the used physical parameters are as follows: $m^* = 0.067 m_0$ (where m_0 is the free electron mass), $\epsilon = 12.58$, $\epsilon_0 = 8.854 \times 10^{-12}$, $e = 1.602 \times 10^{-19}$ C, $\hbar = 1.056 \times 10^{-34}$ Js, $\rho_v = 3 \times 10^{22} \text{ m}^{-3}$, $\Gamma_k = (k = 1, 2, 3)$ is 1, 5 and 7 THz, respectively.

3 Results and discussion

First of all, we try to determine the influences of applied electric (F) and magnetic (B) fields on the total confinement potential, the lowest four energy levels, and their corresponding probability densities as shown in Fig. 1a–c). In Fig. 1a, there is no applied external field on the heterostructure ($F = 0, B = 0$). In this case, it can be easily seen that the wave functions of the ground state, the first excited state, and the second excited state are localized in the left, middle, and right wells, respectively. The wave function of the third excited state is spread over the entire structure due to the weaker confinement compared to other energy levels.

While the external magnetic field is zero, the value of an external electric field is taken as 20 kV/cm in Fig. 1b. Depending on the applied electric field' effect, the shape of confinement potential varies with bending its left side. The energy levels of ground (E_0) and the third excited states (E_3) decrease. The decrease in E_0 is more pronounced. Besides, the first excited state (E_1) and the second excited state (E_2) energy levels have small increases. The energy differences between E_0 and E_1, E_2 , and E_3 have been increased with the variations that occurred in these energy levels. When only the magnetic field ($B = 10T$) is applied to the structure, a parabolic confinement resulting from the squared term of Eq. (1) and a rising in potential barriers occur (Fig. 1c). This effect is the reason of reaching of the energy levels higher values.

The effects of the applied electric and magnetic fields on the structure on the variations of the transition energies between the ground and the first, second, and third excited states are introduced in Fig. 2a, b separately. As seen from Fig. 2a, the increment in the intensity of the electric field (for $B = 0$) creates an increase in the intersubband transition energies. The variation in transition energy (E_{10}) between E_0 and E_1 is greater than the other two transition energies' changes ($E_{20}/2$ and $E_{30}/3$) and it shows a linear increase. In addition to this, in the case of increasing the magnitude of the applied magnetic field (for $F = 0$), the values of E_{10} , $E_{20}/2$, and $E_{30}/3$ reduce. The clearest change occurred in E_{10} .

Fig. 1 The confinement potential, the lowest four energy levels and their probability densities of the heterostructure in the case of (a) applied no external fields ($F = 0, B = 0$), (b) applied only electric field ($F = 20 \text{ kV/cm}, B = 0$), and (c) applied only magnetic field ($F = 0, B = 10T$)

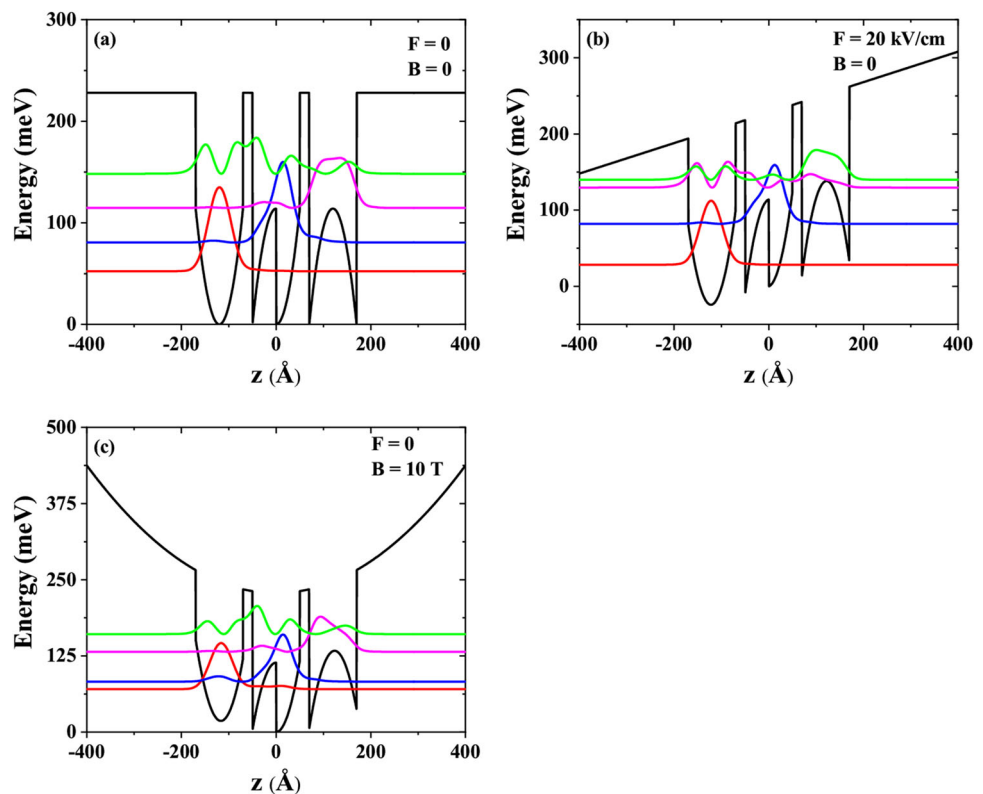


Fig. 2 The changes in the transition energies (E_{10} , $E_{20}/2$, $E_{30}/3$) between the ground state (E_0) and the first, second, and third excited states (E_1 , E_2 , E_3) as a function of the (a) electric field under zero magnetic field and (b) magnetic field under zero electric field

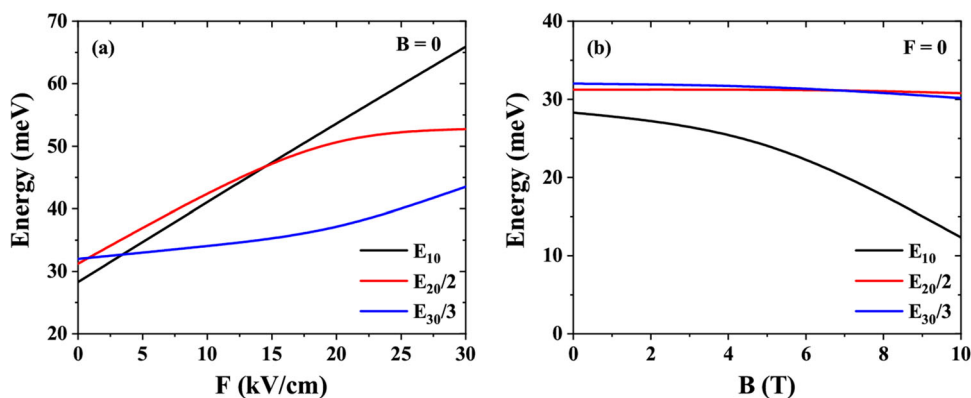


Fig. 3 The variations of the dipole moment matrix elements required to calculate NOR, SHG and THG coefficients as a function of the a electric field and b magnetic field

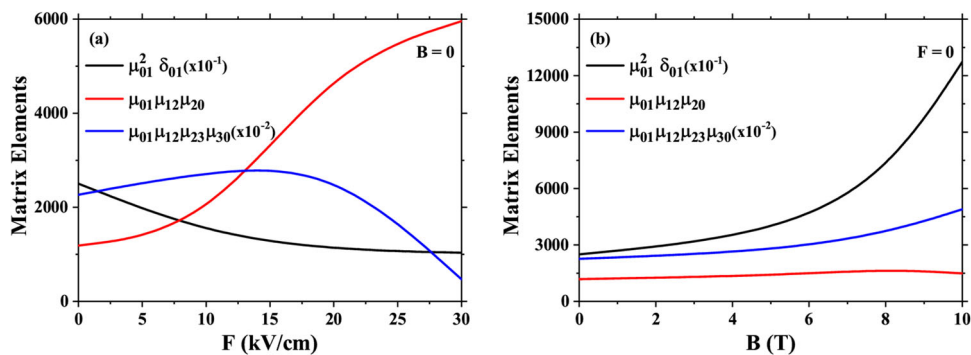


Fig. 4 The variations of NOR coefficient as a function of incident photon energy for different (a) applied electric field (F) intensities and (b) applied magnetic field (B) intensities

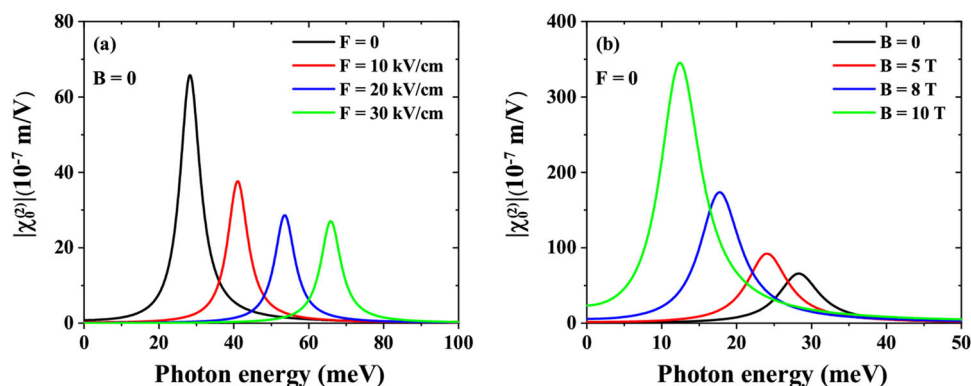


Figure 3 gives how the transition matrix elements in NOR, SHG, and THG coefficients vary with increasing applied external fields. While the applied electric field’s intensity increases, the values of $\mu_{01}^2 \delta_{01}$ ($\mu_{01} \mu_{12} \mu_{20}$) decreases (increases) (Fig. 3a). In the same figure, if the variation of $\mu_{01} \mu_{12} \mu_{23} \mu_{30}$ is examined, it can be seen that firstly it shows an increase from 0 to nearly 15 kV/cm and a decrease from that point. With increasing the applied magnetic field, while the values of $\mu_{01}^2 \delta_{01}$ and $\mu_{01} \mu_{12} \mu_{23} \mu_{30}$ increase, the matrix element $\mu_{01} \mu_{12} \mu_{20}$ increases up to 8 T and then shows a decrease (Fig. 3b).

In Fig. 4, the coefficients of nonlinear optical rectification (NOR) are plotted as a function of incident photon energies for different applied electric and magnetic fields’ intensities. During this examination, firstly we changed the values of electric field intensity from 0 to 30 kV/cm in increments of 10 kV/cm under $B = 0$ (Fig. 4a) and then we took the values of the applied magnetic field as 0, 5T, 8T, 10T for $F = 0$ (Fig. 4b). We have determined that NOR coefficient’s resonance peak shifts to a high energy region (blueshift) by reducing the amplitude with increasing the electric field’s intensity, while it has a redshift (low energy region) by rising the amplitude with increasing the magnetic field’s intensity. If the behaviors of E_{10} and $\mu_{01}^2 \delta_{01}$ from Figs. 2 and 3, respectively for both cases considered here are investigated, it can easily be seen that they support the shifts and amplitude changes that take place here.

After we obtained the NOR coefficient’s variations, we investigated the alterations in SHG coefficient as a function of incident photon energies by changing applied external fields in Fig. 5. We made use of the conditions mentioned in Fig. 4. In Fig. 5a when applied electric field is raised, the peak positions of the SHG coefficient have a blueshift depending on the behavior of the value of $E_{20}/2$ as seen from Fig. 2a. The SHG peaks’ amplitudes increase for the intensities of 10 kV/cm and 20 kV/cm electric field.

Fig. 5 SHG coefficient's change as a function of incident photon energy for different values of the (a) applied electric field (F) and (b) applied magnetic field (B)

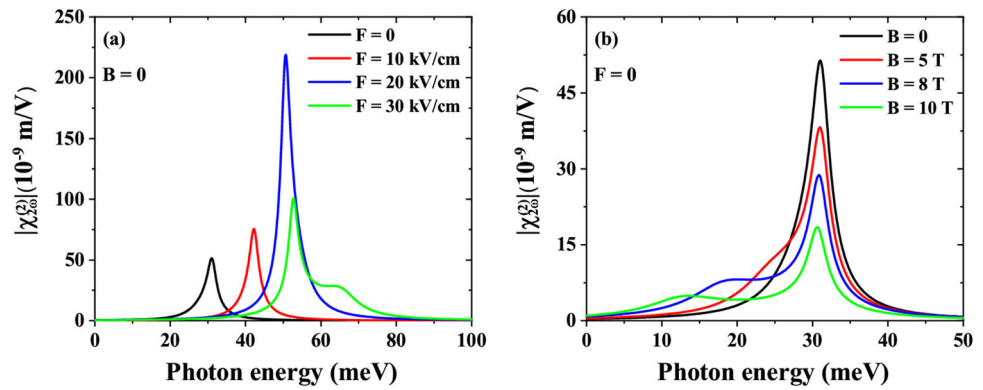
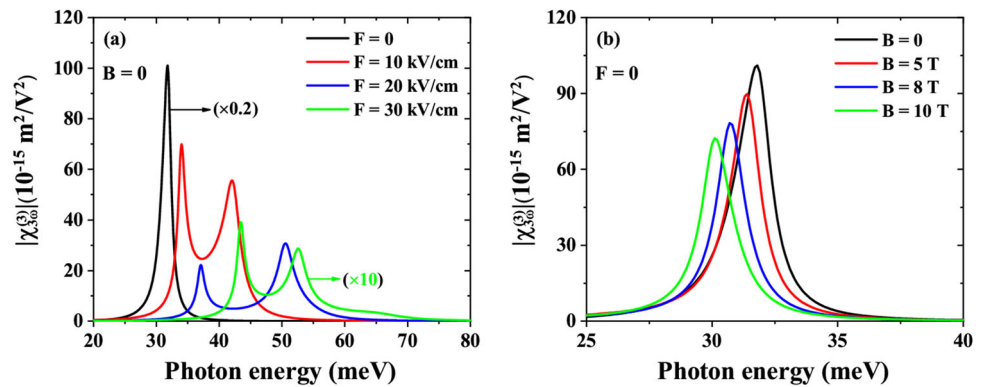


Fig. 6 The variations of THG coefficient as a function of incident photon energy for different intensities of the applied (a) electric field (F) and (b) magnetic field (B)



When the electric field's intensity is 30 kV/cm the SHG peak shows a decrease. To understand the reason for this, Eq. (4), Figs. 2a and 3a must be examined together very carefully. According to Eq. (4), although the transition energy $E_{20}/2$ is responsible for the resonance peak position, not only $\mu_{01}\mu_{12}\mu_{20}$ but also $\mu_{01}\mu_{12}\mu_{20}$, E_{10} and $E_{20}/2$ have a combined effect on the amplitude. The values of E_{10} and $E_{20}/2$ show increments with rising in electric field value (Fig. 2a), while a high increase in $\mu_{01}\mu_{12}\mu_{20}$ is observed (Fig. 3a). These changes cause to increase the numerator and denominator values of Eq. (4). The amplitude shows growth behavior as the increase in the matrix element ($\mu_{01}\mu_{12}\mu_{20}$) is more dominant. However, since there are two peaks in the electric field value of 30 kV/cm, the amplitude value decreased.

The effects of the variations of applied magnetic field on SHG coefficients are studied in Fig. 5b. We have determined that a redshift has occurred in this case. Because of the values of $E_{20}/2$ show very little change as seen from Fig. 2b, the amount of shift here is also not very obvious. The amplitudes of peaks decrease with redshift. We can explain this decrease by analyzing Eq. (4), Figs. 2b and 3b. In the case of magnetic field's intensity increase, while E_{10} shows a more pronounced decrease $E_{20}/2$ has a slight decrease (Fig. 2b). On the other hand, the matrix element $\mu_{01}\mu_{12}\mu_{20}$ tends to decrease, although it shows a slight increase (Fig. 3b). These changes in E_{10} , $E_{20}/2$ and $\mu_{01}\mu_{12}\mu_{20}$ cause to decrease both the numerator and denominator values of the expression in Eq. (4). With the change in E_{10} being more pronounced, the decrease in the denominator becomes more dominant and the amplitudes show decreasing behavior.

In the last examination of our work, we plotted the THG coefficient against incident photon energy in Fig. 6. We investigated the variations of the THG coefficient for the different electric and magnetic fields applied separately. In Fig. 6a, while the magnetic field's intensity is taken as zero, the electric field's intensity is varied as 0, 10 kV/cm, 20 kV/cm, and 30 kV/cm. Despite the THG coefficient have three resonant peaks, two peaks (main and secondary peaks) corresponding to $E_{30}/3$ and $E_{20}/2$, respectively, are given in Fig. 6a. The peak related to E_{10} is too small. The secondary peaks appeared for the values of the electric field different from zero. We can easily see that the main and the secondary resonance peaks of the THG coefficient present a blue shift behavior consistent with the increase in $E_{30}/3$ and $E_{20}/2$, respectively, in Fig. 2a. Similar to the explanations we made for Figs. 4 and 5, we can examine the changes in the expressions in the numerator and denominator in Eq. (5) in order to clarify the amplitude change. E_{10} , $E_{20}/2$ and $E_{30}/3$ values increase in the case of rising electric field (Fig. 2a). At the same time, the matrix element $\mu_{01}\mu_{12}\mu_{23}\mu_{30}$ first shows a slight increase and then a sharper decrease (Fig. 3a). Due to these changes, the numerator and denominator expressions in Eq. (5) decreases and increases, respectively. This result leads to a decrease in amplitudes.

In Fig. 6b, we presented the variations of THG coefficients versus incident photon energy for different intensities of magnetic field (0, 5T, 8T, 10T) under zero electric fields. The peak positions of the THG coefficient move to the lower energy regions with the effect of increasing the magnetic field due to the decrease in the value of $E_{30}/3$ shown in Fig. 2b. As seen from Fig. 5b, as happened in changes of SHG coefficient, the amplitudes of THG peak decline with the increase in the intensity of the applied

magnetic field. While the intensity of magnetic field increase the E_{10} , $E_{20}/2$ and $E_{30}/3$ values decrease (Fig. 2b), this decrease causes to increase the values of the parentheses in the denominator of Eq. (5). In addition to this, we can see from Fig. 3b that the matrix element $\mu_{01}\mu_{12}\mu_{23}\mu_{30}$ in the numerator part of Eq. (5) increases with rising magnetic field. Depending on these changes, the expression in Eq. (5) gets smaller because the increase in the denominator is larger. So the amplitudes of peaks decreases.

4 Conclusions

We analyzed the variations in Nonlinear Optical Rectification (NOR), Second-Harmonic Generation (SHG), and Third-Harmonic Generation (THG) coefficients of $\text{Al}_x\text{Ga}_{1-x}\text{As}/\text{GaAs}$ asymmetric triple QWs structure depending on the applied external fields such as electric and magnetic fields theoretically. The effects of electric and magnetic fields on these nonlinear optical properties were dealt with separately. We utilized the diagonalization and the compact density matrix methods to get subband energy levels (with wave functions) and the mathematical expressions of NOR, SHG, and THG coefficients, respectively. We can summarize our results as follows: while the resonance peaks of the NOR, SHG, and THG coefficients shift to high energy regions with increasing the magnitude of the electric field, they move to the lower energies with increasing the magnitude of the magnetic field. We fully believe that the numerical results we have found will contribute to the development of experimental studies on this subject.

Acknowledgements This research did not receive any specific grant from funding agencies in the public, commercial, or not-for-profit sectors.

Author contributions All the authors have equally contributed to the elaboration of the manuscript.

Data Availability Statement This manuscript has associated data in a data repository. [Authors' comment: The data would be available upon request.]

Declarations

Conflict of interest The authors declare that they do not have any financial and non-financial competing interests.

References

1. S.-H. Lim, Y.-H. Ko, Y.-H. Cho, A quantitative method for determination of carrier escape efficiency in GaN-based light emitting diodes: a comparison of open- and short-circuit photoluminescence. *Appl. Phys. Lett.* **104**, 091104 (2014). <https://doi.org/10.1063/1.4867238>
2. Y. Alahmadi, P. LiKamWa, Effects of selective area intermixing on InAlGaAs multiple quantum well laser diode. *Semicond. Sci. Technol.* **34**, 025010 (2019). <https://doi.org/10.1088/1361-6641/aaf439>
3. H.X. Wang, Z.L. Fu, D.X. Shao, Z.Z. Zhang, C. Wang, Z.Y. Tan, X.G. Guo, J.C. Cao, Broadband bias-tunable terahertz photodetector using asymmetric GaAs/AlGaAs step multi-quantum well. *Appl. Phys. Lett.* **113**, 171107 (2018). <https://doi.org/10.1063/1.5046881>
4. H. Lu, B. Zhang, F. Guo, The photocurrent-voltage characteristic simulated of resonant tunneling photodiodes. *Opt. Quant. Electron.* **48**, 181 (2016). <https://doi.org/10.1007/s11082-016-0373-9>
5. S. Durmuslar, M.E. Mora-Ramos, F. Urgan, Role of external fields on the nonlinear optical properties of a n-type asymmetric δ -doped double quantum well. *Opt. Quantum Electron.* **52**, 495 (2020). <https://doi.org/10.1007/s11082-020-02573-5>
6. E. Kasapoglu, C.A. Duque, M.E. Mora-Ramos, R.L. Restrepo, F. Urgan, U. Yesilgul, H. Sari, I. Sökmen, Combined effects of intense laser field, electric and magnetic fields on the nonlinear optical properties of the step-like quantum well. *Mater. Chem. Phys.* **154**, 170–175 (2015). <https://doi.org/10.1016/j.matchemphys.2015.01.010>
7. C.A. Duque, E. Kasapoglu, S. Sakiroglu, H. Sari, I. Sokmen, Intense laser effects on nonlinear optical absorption and optical rectification in single quantum wells under applied electric and magnetic field. *Appl. Surf. Sci.* **257**, 2313–2319 (2011). <https://doi.org/10.1016/j.apsusc.2010.09.095>
8. H.S. Aydinoglu, M. Sayrac, M.E. Mora-Ramos, F. Urgan, Nonlinear optical properties in $\text{Al}_x\text{Ga}_{1-x}\text{As}/\text{GaAs}$ double-graded quantum wells: the effect of the structure parameter, static electric, and magnetic field. *Solid State Commun.* **342**, 114647 (2022). <https://doi.org/10.1016/j.ssc.2021.114647>
9. J.C. Martinez-Orozco, M.E. Mora-Ramos, C.A. Duque, Nonlinear optical rectification and second and third harmonic generation in GaAs δ -FET systems under hydrostatic pressure. *J. Lumin.* **132**, 449–456 (2012). <https://doi.org/10.1016/j.jlumin.2011.09.022>
10. İ Karabulut, H. Şafak, M. Tomak, Nonlinear optical rectification in asymmetrical semiparabolic quantum wells. *Solid State Commun.* **135**, 735–738 (2005). <https://doi.org/10.1016/j.ssc.2005.06.001>
11. R.-Z. Wang, K.-X. Guo, Z.-L. Liu, B. Chen, Y.-B. Zheng, Nonlinear optical rectification in asymmetric coupled quantum wells. *Phys. Lett. A* **373**, 795–798 (2009). <https://doi.org/10.1016/j.physleta.2008.12.043>
12. S. Shao, K.-X. Guo, Z.-H. Zhang, N. Li, C. Peng, Third-harmonic generation in cylindrical quantum dots in a static magnetic field. *Solid State Commun.* **151**, 289–292 (2011). <https://doi.org/10.1016/j.ssc.2010.12.003>
13. E.B. Al, E. Kasapoglu, F. Urgan, Dynamics of nonlinear optical rectification, second, and third harmonic generation in asymmetric triangular double quantum wells due to static electric and magnetic fields. *Eur. Phys. J. Plus.* **137**, 466 (2022). <https://doi.org/10.1140/epjp/s13360-022-02702-x>
14. O. Aytakin, S. Turgut, M. Tomak, Nonlinear optical properties of a Pöschl-Teller quantum well under electric and magnetic fields. *Phys. E* **44**, 1612–1616 (2012). <https://doi.org/10.1016/j.physe.2012.04.005>
15. M.E. Mora-Ramos, C.A. Duque, E. Kasapoglu, H. Sari, I. Sökmen, Linear and nonlinear optical properties in a semiconductor quantum well under intense laser radiation: effects of applied electromagnetic fields. *J. Lumin.* **132**, 901–913 (2012). <https://doi.org/10.1016/j.jlumin.2011.11.008>
16. X. Liu, L. Zou, C. Liu, Z.-H. Zhang, J.-H. Yuan, The nonlinear optical rectification and second harmonic generation in asymmetrical Gaussian potential quantum well: effects of hydrostatic pressure, temperature and magnetic field. *Opt. Mater.* **53**, 218–223 (2016). <https://doi.org/10.1016/j.optmat.2016.01.043>

17. R.L. Restrepo, E. Kasapoglu, S. Sakiroglu, F. Urgan, A.L. Morales, C.A. Duque, Second and third harmonic generation associated to infrared transitions in a Morse quantum well under applied electric and magnetic fields. *Infrared Phys. Technol.* **85**, 147–153 (2017). <https://doi.org/10.1016/j.infrared.2017.06.005>
18. F. Urgan, M.E. Mora-Ramos, U. Yesilgul, H. Sari, I. Sokmen, Effect of applied external fields on the nonlinear optical properties of a Woods-Saxon potential quantum well. *Phys. E* **111**, 167–171 (2019). <https://doi.org/10.1016/j.physe.2019.03.015>
19. M. Sayrac, J.C. Martínez-Orozco, M.E. Mora-Ramos, F. Urgan, The nonlinear optical rectification, second and third harmonic generation coefficients of Konwent potential quantum wells. *Eur. Phys. J. Plus.* **137**, 1033 (2022). <https://doi.org/10.1140/epjp/s13360-022-03207-3>
20. H. Dakhlaoui, I. Altuntas, M.E. Mora-Ramos, F. Urgan, Numerical simulation of linear and nonlinear optical properties in heterostructure based on triple Gaussian quantum wells: effects of applied external fields and structural parameters. *Eur. Phys. J. Plus.* **136**, 894 (2021). <https://doi.org/10.1140/epjp/s13360-021-01907-w>
21. J.-B. Xia, W.-J. Fan, Electronic structures of superlattices under in-plane magnetic field. *Phys. Rev. B* **40**, 8508 (1989). <https://doi.org/10.1103/PhysRevB.40.8508>
22. F. Urgan, Intensity-dependent nonlinear optical properties in a modulation-doped single quantum well. *J. Lumin.* **131**, 2237 (2011). <https://doi.org/10.1016/j.jlumin.2011.06.003>
23. H.S. Aydinoglu, S. Sakiroglu, H. Sari, F. Urgan, I. Sökmen, Nonlinear optical properties of asymmetric double-graded quantum wells. *Philos. Mag. A* **98**, 2151 (2018). <https://doi.org/10.1080/14786435.2018.1476785>
24. J.C. Martínez-Orozco, J.G. Rojas-Briseño, K.A. Rodríguez-Magdaleno, I. Rodríguez-Vargas, M.E. Mora-Ramos, R.L. Restrepo, F. Urgan, E. Kasapoglu, C.A. Duque, Effect of the magnetic field on the nonlinear optical rectification and second and third harmonic generation in double δ -doped GaAs quantum wells. *Phys. B* **525**, 30–35 (2017). <https://doi.org/10.1016/j.physb.2017.08.082>
25. E. Rosencher, P. Bois, Model system for optical nonlinearities: asymmetric quantum wells. *Phys. Rev. B* **44**, 11315–11327 (1991). <https://doi.org/10.1103/PhysRevB.44.11315>
26. Y.B. Yu, H.J. Wang, Third-harmonic generation in two-dimensional pseudodot system with applied magnetic field. *Superlattice Microstruct.* **50**, 252–260 (2011). <https://doi.org/10.1016/j.spmi.2011.07.001>

Springer Nature or its licensor (e.g. a society or other partner) holds exclusive rights to this article under a publishing agreement with the author(s) or other rightsholder(s); author self-archiving of the accepted manuscript version of this article is solely governed by the terms of such publishing agreement and applicable law.